Chemical Research in Toxicology

Article

pubs.acs.org/crt

Enhancing Bulge Stabilization through Linear Extension of C8-Aryl-Guanine Adducts to Promote Polymerase Blockage or Strand Realignment to Produce a C:C Mismatch

Michael Sproviero,[†] Anne M. R. Verwey,[†] Aaron A. Witham,[†] Richard A. Manderville,*[,†] Purshotam Sharma,[‡,§] and Stacey D. Wetmore*[,‡]

[†]Department of Chemistry and Toxicology, University of Guelph, Guelph, ON Canada N1G 2W1

[‡]Department of Chemistry & Biochemistry, University of Lethbridge, Lethbridge, AB Canada T1K 3M4

Supporting Information

ABSTRACT: Aryl radicals can react at the C8-site of 2′-deoxyguanosine (dG) to produce DNA adducts with a C8−C linkage (denoted C-linked). Such adducts are structurally distinct from those possessing a flexible amine (N-linked) or ether (O-linked) linkage, which separates the C8-aryl moiety from the guanine nucleobase. In the current study, two model C-linked C8-dG adducts, namely, C8-benzo[*b*]thienyl-dG ([BTh]G) and C8-(pyren-1-yl)-dG ([Py]G), were incorporated into the *Nar*I (12mer, *Nar*I(12) and 22mer, *Nar*I(22)) hotspot sequence for frameshift mutations in bacteria. For the first time, C-linked C8-dG adducts are shown to stabilize the −2 deletion duplex within the *Nar*I sequence. Primer-elongation assays employing *Sulfolobus solfataricus* P2 DNA polymerase IV (Dpo4) demonstrates the influence of C8-aryl ring size and shape in promoting Dpo4 blockage or strand realignment to produce a C:C mismatch downstream of the adduct site. Molecular dynamics simulations of the −2 deletion duplex suggest that both *anti* and *syn* adduct structures are energetically accessible. These findings provide a rationale for describing the biochemical outcome induced by C-linked C8-dG adducts when processed by Dpo4.

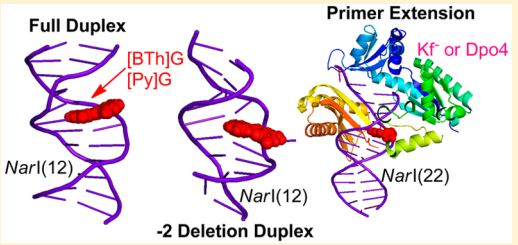

INTRODUCTION

Aromatic compounds can undergo enzymatic transformations to generate highly reactive electrophiles that covalently attach to DNA to produce bulky DNA adducts (addition products). The resulting adducts can cause genetic changes that play an important role in the etiology of cancer.[1] Bulky adducts formed at the C8-site of 2′-deoxyguanosine (dG) are among the most common lesions produced by chemical carcinogens.[2] Aromatic amines,[3] nitroaromatics,[4] and food-borne heterocyclic amines[5] have been implicated in human cancers and undergo metabolic activation to afford nitrenium ions that produce C8-dG adducts containing a C8-N-aryl linkage (denoted N-linked adducts).[6,7] Other aromatic mutagens, such as aryl hydrazines,[8,9] estrogens,[10,11] polycyclic aromatic hydrocarbons (PAHs),[12,13] and phenols[14,15] may be enzymatically transformed to yield radical species that react directly at the C8-site of dG to produce a C8-C linkage (denoted C-linked adducts, Figure 1).[16] Phenolic toxins can also generate O-linked C8-dG adducts (containing an ether C8−O−C linkage)[17,18] due to the ambident reactivity (C- vs O-attack) of the phenoxyl radical.[19]

To understand the biological impact of bulky DNA adducts, efforts have been made to relate the adducted duplex structures to mutagenic outcome. For the N-linked C8-dG adducts, major conformational motifs in duplex DNA (i.e., the major groove B-type,[20] the base-displaced stacked (S-type),[21,22] and the minor groove wedge (W-type)[23−25]) have been characterized by NMR spectroscopy. The distribution among the various conformations is dependent on the nature of the attached C8-moiety and the neighboring base sequence contexts.[26] In general, N-linked C8-dG adducts that exhibit potent mutagenicity favor the *syn*-conformation to generate the S-type or W-type duplexes.

C-Linked C8-dG adducts lack a flexible tether separating the aryl component from the dG base, which reduces the inherent conformational flexibility of the lesion and alters it is orientation in the DNA duplex.[27−29] Recently, we examined the structural and biochemical impact of a series of C-linked adducts (viz., C8-aryl = furyl ([Fur]G), phenyl ([Ph]G), and quinolyl ([Q]G); Figure 1) differing in aryl ring size.[27] The adducts were incorporated into the G3-position (X) of the *Nar*I sequence (Figure 1), which is part of a CG dinucleotide repeat and has been shown to be a hotspot for two-base deletion mutations induced by polycyclic N-linked C8-dG adducts in bacteria[30] via a two-base slippage mechanism.[31] Within the *Nar*I(12) duplex, the C-linked adducts adopted the B-type structure opposite C. When the modified *Nar*I(12) sequences were hybridized with a truncated 10-mer sequence (−2), which produces a 2-base bulge aimed at mimicking a slipped mutagenic intermediate,[32−34] none of the lesions stabilized the truncated duplex, suggesting an inability to induce −2 deletion mutations.[27] Primer-elongation assays were carried out

Received: June 4, 2015
Published: July 30, 2015

DOI: 10.1021/acs.chemrestox.5b00233
Chem. Res. Toxicol. 2015, 28, 1647−1658

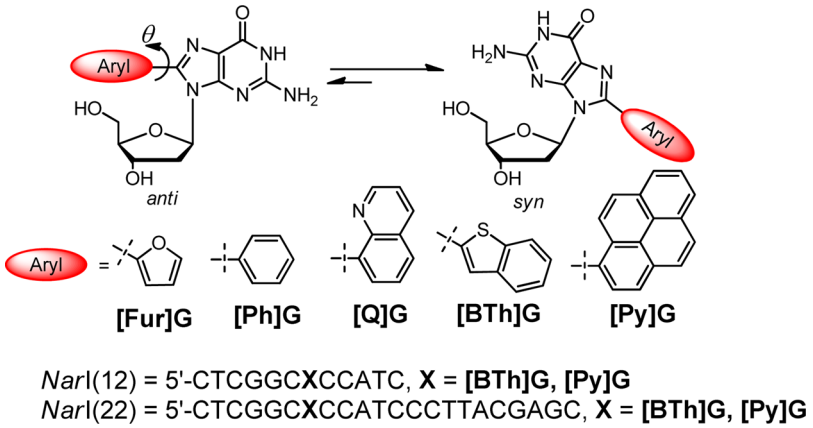

Figure 1. Structures of C-linked C8-dG adducts, oligonucleotide sequences of *Nar*I(12) and *Nar*I(22), and torsion angle θ at the C8-linkage.

using the *Nar*I(22) template (Figure 1) annealed to a 15mer primer in the presence of the Klenow fragment exo$^-$ (Kf$^-$) or the Y-family DNA polymerase IV (Dpo4) from *Sulfolobus solfataricus*. Single-nucleotide incorporation assays revealed that the smallest adduct [Fur]G generated the greatest levels of base misincorporation.[27] The C-linked adducts also induced slippage by Dpo4 to create a C:C mismatch distal to the adduct site.

In the present study, new aspects of the structural and biochemical impact of C-linked C8-dG aryl ring size and shape are unveiled by exploring the C8-benzo[*b*]thienyl-dG ([BTh]G)[35] and C8-(pyren-1-yl)-dG ([Py]G)[36,37] (Figure 1) adducts. Specifically, the adducts were incorporated into the *Nar*I sequence to determine their structural preferences within *Nar*I(12) and the subsequent impact on primer-elongation within the *Nar*I(22) template. The aryl ring of [BTh]G represents a linear phenyl extension of furyl in [Fur]G (and difference in the heterocycle, S vs O), while the pyrene moiety in [Py]G linearly extends the quinolyl in Q[G] by a naphthyl group. Both [BTh]G[35] and [Py]G[36] exhibit fluorescence in the single-strand that is sensitive to hybridization for predicting adduct conformation within duplex DNA. The [Py]G adduct has previously been incorporated into an oligonucleotide substrate for primer extension analysis using Kf$^-$ and Dpo4.[37] However, [Py]G was inserted into a noniterated sequence in which it was not possible for [Py]G to induce polymerase slippage. Thus, it is of interest to consider the impact of [Py]G within the *Nar*I template for comparison to other C-linked adducts with various ring sizes (Figure 1). For the first time, our studies demonstrate that polycyclic C-linked C8-dG adducts can stabilize the −2 deletion duplex within the *Nar*I sequence. However, unlike the N-linked C8-dG counterparts that promote slippage to afford dinucleotide deletion in primer-elongation assays, slippage mediated by C-linked C8-dG adducts is accompanied by either polymerase blockage or strand realignment to produce a C:C mismatch.

EXPERIMENTAL PROCEDURES

Materials. Boronic acids (benzo[*b*]thien-2-ylboronic acid and pyrene-1-boronic acid), $Pd(OAc)_2$, 3,3′,3″-phosphinidynetris-(benzenesulfonic acid) trisodium salt (TPPTS), *N*,*N*-dimethylformamide diethyl acetal, 4,4′-dimethoxytrityl chloride, 2-cyanoethyl *N*,*N*-diisopropyl-chlorophosphoramidite, and other commercial products used for the synthesis of [Bth]G and [Py]G phosphoramidites were used as received. Unmodified oligonucleotides (*Nar*I(12), *Nar*I(22), complementary strands for *Nar*I(12), 15mer, and other primers) were purchased from Sigma Genosys and were purified by Sigma using polyacrylamide gel electrophoresis. *Escherichia coli* pol I Klenow fragment exo− (Kf$^-$) and T4 polynucleotide kinase were purchased from NewEngland BioLabs, while *Sulfolobus solfataricus* P2 DNA polymerase IV (Dpo4) was purchased from Trevigen Inc. Isotopically labeled ATP ([γ-^{32}P]-ATP) was purchased from PerkinElmer.

Methods. Suzuki cross-coupling reactions of boronic acids with 8-Br-dG to afford [BTh]G and [Py]G were performed as described previously by Western and co-workers.[38] NMR spectra were recorded on 300 and 600 MHz Bruker spectrometers in acetone-d_6, $CDCl_3$, CD_2Cl_2, or DMSO-d_6 referenced to TMS (0 ppm), or the respective solvent. Full synthetic details of modified phosphoramidites, NMR spectra, and ESI-MS analysis of modified *Nar*I oligonucleotides are available in Supporting Information (SI). All adducted *Nar*I(12) and *Nar*I(22) oligonucleotide substrates were prepared on a 1 μmol scale using a BioAutomation MerMade 12 automatic DNA synthesizer using standard or modified β-cyanoethylphosphoramidite chemistry. All melting temperatures (T_m) of *Nar*I(12) oligonucleotides were measured using a Cary 300-Bio UV−vis spectrophotometer equipped with a 6 × 6 multicell Peltier block-heating unit using Hellma 114-QS 10 mm light path cells. Oligonucleotide samples were prepared in 50 mM phosphate buffer, pH 7, with 100 mM NaCl, using equivalent amounts (6.0 μM) of the unmodified or C8-aryl-dG modified *Nar*I(12) oligonucleotide and its complementary strand. The T_m values of the duplexes were determined as previously outlined.[27] Circular dichroism (CD) spectra were recorded on a Jasco J-815 CD spectropolarimeter equipped with a 1 × 6 Multicell block thermal controller and a water circulator unit. Measurements were carried out in 50 mM phosphate buffer, pH 7, with 100 mM NaCl, using equivalent amounts (6.0 μM) of the unmodified or C8-aryl-G modified *Nar*I(12) oligonucleotide and its complementary strand. Spectra were collected at 10 °C between 200 and 400 nm, with a bandwidth of 1 nm and scanning speed at 100 nm/min, as previously described.[27] All fluorescence spectra were recorded on a Cary Eclipse Fluorescence spectrophotometer equipped with a 1 × 4 Multicell block Peltier stirrer and temperature controller. *Nar*I(12) samples were prepared in 50 mM phosphate buffer, pH 7, with 100 mM NaCl. In each case, both excitation and emission spectra were recorded for the C8-aryl-G modified *Nar*I(12) oligonucleotide hybridized to its complementary strand at 10 °C. Computational methods are available in SI, and the followed strategies have been previously outlined.[27−29] Full details of the primer-elongation experiments are also provided in SI and the followed protocols have been previously described.[18,27,39]

RESULTS

***Nar*I(12) Properties.** *UV Thermal Melting.* Solid-phase DNA synthesis was employed to incorporate the C8-dG adducts ([BTh]G and [Py]G) into the G3-position (X) of *Nar*I(12) (Figure 1, see Figures S1−S14 for synthetic details and electrospray ionization (ESI) MS spectra of adducted oligonucleotides (Table S1 and Figures S15−S18). UV−vis thermal melting parameters for the [BTh]G- and [Py]G-

DOI: 10.1021/acs.chemrestox.5b00233
Chem. Res. Toxicol. 2015, 28, 1647−1658

modified *Nar*I(12) duplexes are summarized in Table 1. The adducts strongly decreased duplex stability when paired

Table 1. Thermal Melting Parameters of C8-aryl-dG modified *Nar*I(12)

5′-CTC-GGC-X-CCA-TC-3′				5′-CTC-GG-CX-CCA-TC-3′			
3′-GAG-CCG-N-GGT-CT-5′				3′-GAG-CC----GGT-AG-5′(-2)			
X	N	T_m (°C)[a]	ΔT_m[b]	X	N	T_m (°C)[a]	ΔT_m[b]
G	C	63.6	–	G	THF	45.7	–
[BTh]G	C	47.8	−15.8	[BTh]G	THF	50.1	+4.4
[Py]G	C	43.5	−20.1	[Py]G	THF	45.3	−0.4
G	G	54.0	–	G	−2	39.4	–
[BTh]G	G	54.9	+0.9	[BTh]G	−2	43.2	+3.8
[Py]G	G	49.0	−5.0	[Py]G	−2	45.6	+6.2

[a] T_m values of duplexes (6.0 μM) measured in 50 mM sodium phosphate buffer, pH 7, with 0.1 M NaCl and a heating rate of 1 °C/min; errors are ±1 °C. [b] ΔT_m = T_m (modified duplex) − T_m (unmodified duplex).

opposite C (i.e., ΔT_m = −15.8 °C for [BTh]G and −20.1 for [Py]G). Paired opposite G, [BTh]G had a slight stabilizing influence compared to that of the unmodified G:G mismatch (i.e., ΔT_m = +0.9 °C), while [Py]G decreased duplex stability (ΔT_m = −5.0 °C). However, the T_m values for the C-linked adducts paired opposite G were considerably greater than the T_m's opposite C (i.e., 54.9 vs 47.8 °C for [BTh]G and 49.0 vs 43.5 °C for [Py]G).

The C8-dG adducts were also paired opposite the stable tetrahydrofuran (THF) model of an abasic site[40] to assess the influence of π-stacking interactions in the absence of H-bonding with an opposing base. The [BTh]G adduct increased duplex stability (i.e., ΔT_m = +4.4 °C), while [Py]G had little influence on duplex stability compared to that of the unmodified control (i.e., ΔT_m = −0.4 °C). The adducted *Nar*I(12) strands were also hybridized with the truncated 10-mer sequence (−2) to generate a −2 deletion duplex that models the slipped mutagenic intermediate.[32−34] Enhanced stability of the truncated duplex is believed to correlate with an ability to promote −2 frameshift mutagenesis in bacteria. For example, the N-linked C8-dG adduct of *N*-acetyl-2-aminofluorene ([AAF]G) is a potent frameshift mutagen in bacteria and affords a ΔT_m value of +15 °C for the truncated duplex in 0.1 M NaCl.[32,33] Both [BTh]G and [Py]G stabilized the −2 deletion duplex compared with that of the unmodified control, exhibiting ΔT_m values of +3.8 and +6.2 °C, respectively. For [Py]G, the T_m of the truncated duplex was greater than the T_m of the full-length complement (45.6 vs 43.5 °C), while for [BTh]G, the T_m was slightly diminished (43.2 vs 47.8 °C). These findings contrast with our previous results with the single-ringed derivatives ([Fur]G, Ph[G]) and the bent fused-ringed system in [Q]G, which failed to stabilize the −2 deletion duplex.[27]

Circular Dichroism. The *Nar*I(12) duplexes were analyzed using CD spectroscopy (Figure 2) to determine the impact of the adduct on the global tertiary structures. All duplexes showed CD characteristics for a B-DNA helical conformation, with positive (275 nm) and negative (244 nm) S-shaped CD curves with a crossover at approximately 260 nm (Figure 2).[41] A dominant feature of the CD curves was the induced circular

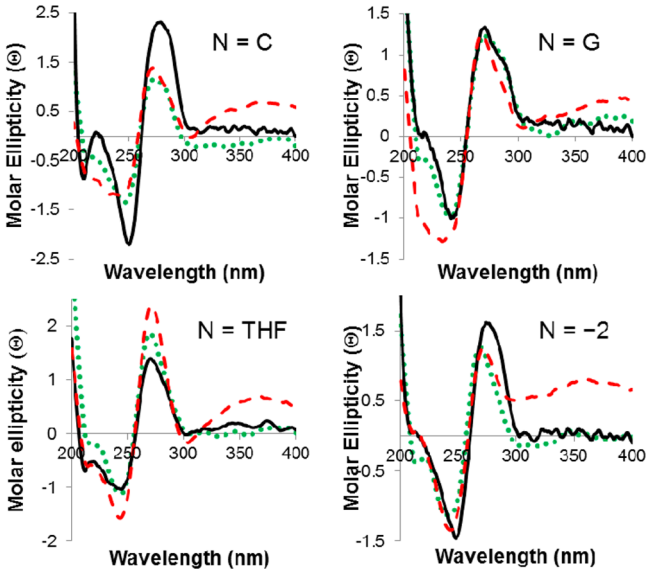

Figure 2. CD spectral overlays of *Nar*I(12) duplexes with X = G (solid black lines), X = [BTh]G (dotted green lines), and X = [Py]G (dashed red lines). All spectra of duplexes (6 μM) were recorded in 50 mM sodium phosphate buffer, pH 7, with 0.1 M NaCl at 10 °C.

dichroism in the 300−400 nm range ($ICD_{300-400\ nm}$) for the [Py]G-modified *Nar*I(12) duplexes (dashed red traces). All [Py]G-modified *Nar*I(12) duplexes exhibited a positive $ICD_{300-400\ nm}$, while the [BTh]-modified and control NarI(12) duplexes did not exhibit ICD. For the N-linked 2-aminofluorene-dG adduct ([AF]G), the Cho laboratory has previously demonstrated that positive ICD in the 290−360 nm range is a sensitive conformational marker for [AF]G-induced S/B heterogeneity in the fully paired *Nar*I-dC duplexes.[42] Thus, the CD data for [Py]G-modified *Nar*I(12) paired opposite C was consistent with the presence of the S-conformation. The positive $ICD_{300-400\ nm}$ in the other [Py]G-modified *Nar*I(12) duplexes (N = G, THF and −2) suggested a *syn*-conformational preference for [Py]G, which places the pyrene moiety in the chiral helical environment.

Fluorescence. Changes in the fluorescent properties of [BTh]G and [Py]G in the single-strand *Nar*I(12) versus the duplex structures were also examined to probe conformational preferences (Table 2). Both [BTh]G[35] and [Py]G[36] exhibit fluorescence in the single-strand that is sensitive to hybridization. For example, in the single-strand, [BTh]G exhibited λ_{ex} = 321 nm and λ_{em} = 416 nm that shifted to λ_{ex} = 330 nm ($\Delta\lambda_{ex}$ = 9 nm) and 415 nm ($\Delta\lambda_{em}$ = −1 nm) in the duplex with [BTh]G paired opposite THF. A more dramatic fluorescence response was observed for [Py]G paired opposite THF, in which the fluorescence shifted from λ_{ex} = 351 nm and λ_{em} = 456 nm in the single-strand to λ_{ex} = 371 nm ($\Delta\lambda_{ex}$ = 20 nm) and λ_{em} = 453 nm ($\Delta\lambda_{em}$ = −3 nm) in the duplex. The 20 nm red-shift in λ_{ex} upon hybridization with the N = THF complementary strand indicates a strong stacking interaction of the pyrene moiety with adjacent base pairs inside the duplex.[36] The λ_{em} exhibits a blue-shift because the C8-aryl moiety is sequestered from the polar aqueous solvent environment.[27,36] For [Py]G paired opposite C, G, and −2, λ_{ex} also shifted to the red, but to a lesser degree (10−11 nm), while λ_{em} displayed small changes (+1, −3 nm). Overall, the fluorescence response of [Py]G within *Nar*I(12) to duplex formation suggested the involvement of a *syn*-conformation,

DOI: 10.1021/acs.chemrestox.5b00233
Chem. Res. Toxicol. 2015, 28, 1647−1658

Table 2. Photophysical Parameters of C8-aryl-dG Modified *Nar*I(12)

X	N	λ_{ex} (nm)[a]	$\Delta\lambda_{ex}$ (nm)[b]	λ_{em} (nm)	$\Delta\lambda_{em}$ (nm)	$\Delta\nu$ (cm^{-1})[c]	I_{rel} (em)[d]
[BTh]G	/[e]	321	/	416	/	7114	/
[BTh]G	C	334	13	423	7	6299	1.45
[BTh]G	G	326	5	415	−1	6578	0.67
[BTh]G	THF	330	9	415	−1	6677	0.58
[BTh]G	−2	323	2	413	−3	6747	1.05
[Py]G	/	351	/	456	/	6560	/
[Py]G	C	361	10	455	−1	5723	0.85
[Py]G	G	362	10	457	1	5743	0.61
[Py]G	THF	371	20	453	−3	4879	0.97
[Py]G	−2	362	11	453	−3	5549	0.61

[a]All spectra of single-strand *Nar*I(12) and duplexes (6 μM) were recorded in 50 mM sodium phosphate buffer, pH 7, with 0.1 M NaCl at 10 °C. [b]Change in excitation or emission maximum for duplex versus single-strand. [c]Stokes' shift ($\Delta\nu$) is calculated as $(1/\lambda_{ex} - 1/\lambda_{em})$. [d]$I_{rel} = I_{duplex}/I_{single\text{-}strand}$. [e]$N$ = / indicates the optical properties of the modified base in the single-strand.

which is consistent with the positive $ICD_{300-400\ nm}$ in the CD spectra (Figure 2). In contrast, [BTh]G paired opposite C exhibited a significant red-shift in both λ_{ex} ($\Delta\lambda_{ex}$ = 13 nm) and λ_{em} ($\Delta\lambda_{em}$ = 7 nm). The red-shift in emission for [BTh]G upon base-pairing to C suggested placement of the modified base in a polar environment, which is consistent with the formation of the B-type structure.[35] For [BTh]G paired opposite G and −2, the emission exhibited small blue-shifts (−1−3 nm), as noted for [BTh]G paired opposite THF, suggesting the involvement of the *syn*-conformation.[35]

Molecular Dynamics (MD) Simulations. MD simulations were carried out on the (*anti* or *syn*) [BTh]G and [Py]G adducts at the G3-position in the *Nar*I(12) sequence opposite C, G, THF, or −2, and the resulting conformations were ranked according to the calculated free energies (see Section S1, SI for a detailed discussion,).

Adducts Paired against C. The major groove (B-type) and wedge (W-type) conformations are energetically accessible (i.e., within 25 kJ mol^{-1}) for [BTh]G-adducted DNA (Figure 3 and Table S3) as the smaller benzothiophene moiety renders the base displaced intercalated (S-type) conformation energetically inaccessible. There is a small energetic separation between the B-type and S-type conformations for [Py]G adducted DNA (Table S3). The *syn* conformer completely intercalates the pyrene moiety into the helix (Figure 3), which displaces both the damaged G and the opposing C into the major groove (Figure S28). The accessibility of the S-type conformation of [Py]G-adducted DNA is supported by the induced CD band resulting from the *syn*-orientation and stacking of the pyrene moiety in *Nar*I damaged DNA against C (Figure 2). Similarly, the absence of the induced CD band for [BTh]G-adducted DNA correlates with the lack of stacking with the C8-moiety and the energetic accessibility of only the B-type and W-type conformations.

Adducts Paired against G. Against G, *syn* [BTh]G and [Py]G were paired against *anti*-G, while the *anti* adducts were paired against *syn*-G, to allow Hoogsteen hydrogen bonding. [BTh]G-adducted DNA prefers the *syn* adduct conformations (Figure 4 and Table S3). In contrast, the [Py]G adduct likely adopts a mixture of the hydrogen bonded *anti* and stacked *syn* conformers, with the greatest stabilization exhibited for the *syn*-conformations (Figure S30 and Table S3). The accessibility of both orientations may explain why DNA containing [Py]G against G leads to a weaker ICD band compared to the corresponding ICD for [Py]G paired against C (Figure 2). In addition, the absence of hydrogen bonding with the adduct in the dominant *syn*-conformation may explain why [Py]G-adducted DNA shows decreased melting temperatures compared to those of the unmodified control (Table 1).

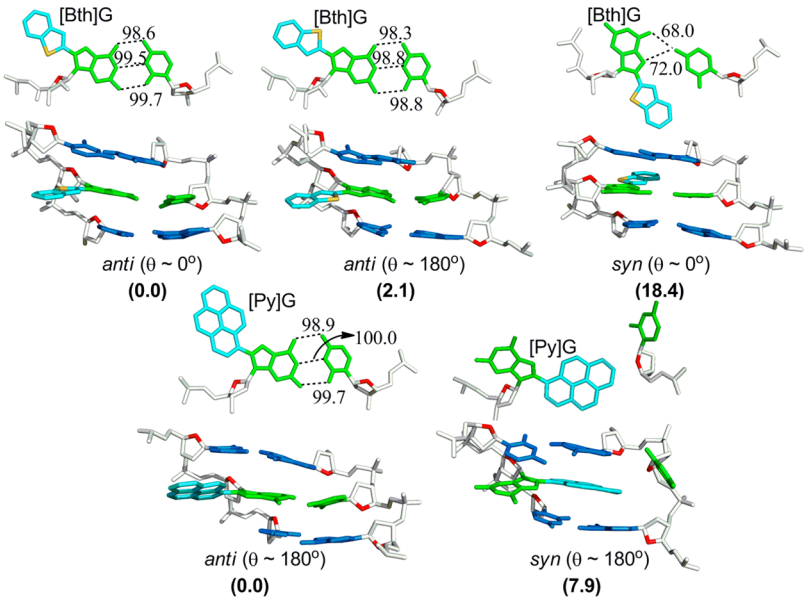

Figure 3. Representative structures corresponding to the most stable (within 25 kJ mol^{-1}) *anti* and *syn* conformations for the studied adducts paired against C. The relative free energies (kJ mol^{-1}) of competing conformations for each adduct are provided in bold. The corresponding orientation of the damaged base pair is explicitly shown for each conformation. H-bonding contacts are indicated by dashed lines with percent occupancies calculated using a donor−acceptor (X−Y) distance cutoff of 3.4 Å and X−H···Y angle cutoff of 120°. Data are provided only for those H-bonds that persist for more than 15% of the simulation time.

DOI: 10.1021/acs.chemrestox.5b00233
Chem. Res. Toxicol. 2015, 28, 1647−1658

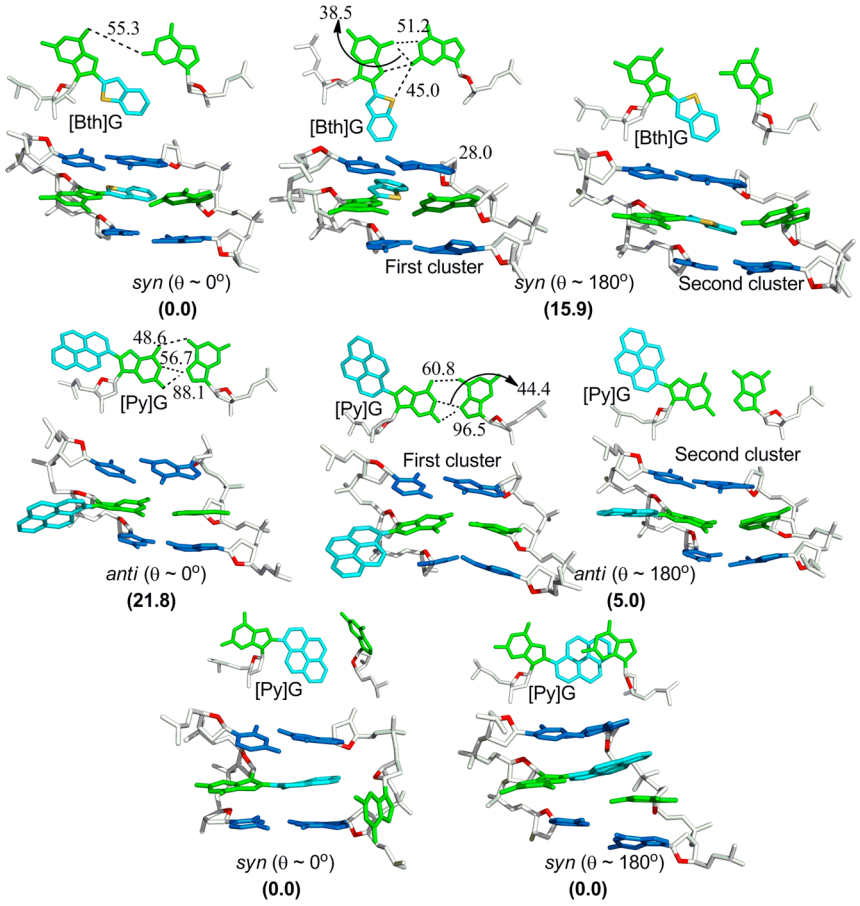

Figure 4. Representative structures corresponding to the most stable (within 25 kJ mol^{-1}) *anti* and *syn* conformations for the studied adducts paired against G. The relative free energies (kJ mol^{-1}) of competing conformations for each adduct are provided in bold. The corresponding orientation of the damaged base pair is explicitly shown for each conformation. H-bonding contacts are indicated by dashed lines with percent occupancies calculated using a donor−acceptor (X−Y) distance cutoff of 3.4 Å and X−H···Y angle cutoff of 120°. Data are provided only for those H-bonds that persist for more than 15% of the simulation time. For simulations with more than one cluster of structures, H-bond contacts and occupancies for the total simulation time are displayed on one of the clusters.

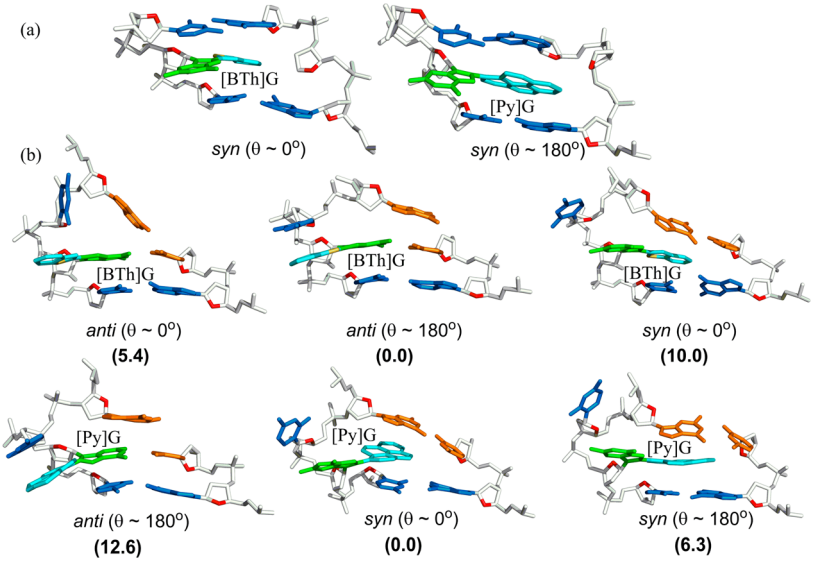

Figure 5. Representative structures corresponding to the most stable (within 25 kJ mol^{-1}) *anti* and *syn* conformations for the studied adducts paired against (a) THF and (b) the −2 base bulge. The relative free energies (kJ mol^{-1}) of competing conformations for each adduct are provided in bold.

Adducts Paired against THF. The *anti*-conformers are energetically inaccessible to both [BTh]G and [Py]G paired opposite THF (Table S3). In the favored *syn*-conformers, the C8-moiety intercalates into the helix and thereby pushes the

DOI: 10.1021/acs.chemrestox.5b00233
Chem. Res. Toxicol. 2015, 28, 1647−1658

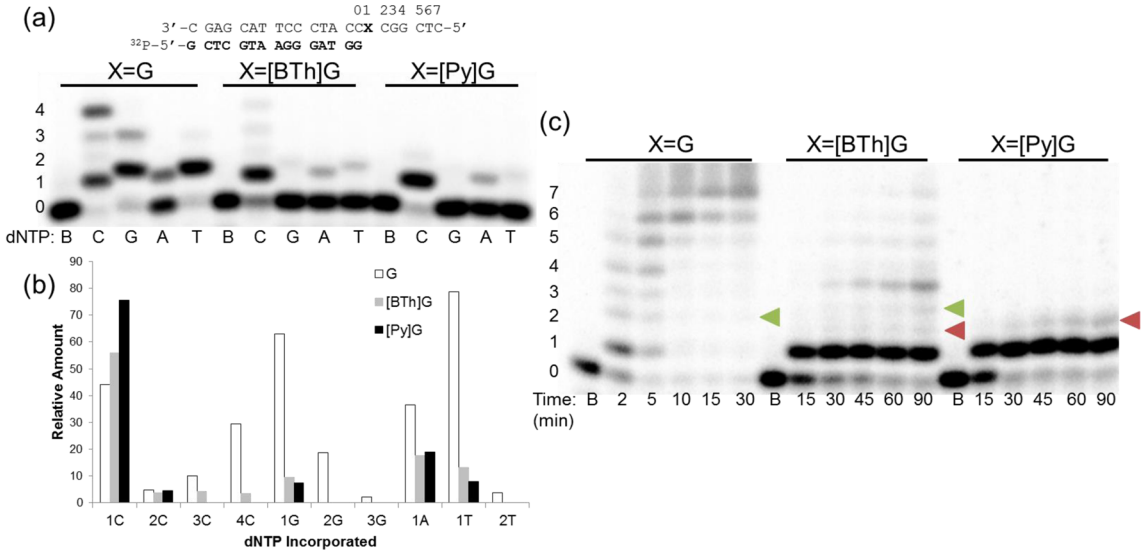

Figure 6. (a) Primer-extension of *Nar*I(22):15mer duplex (100 nM, X = G, [BTh]G or [Py]G) by Dpo4 (20 nM) in the presence of individual dNTPs (indicated under each lane, 25 μM). Reactions were incubated at 37 °C for 30 min. (b) Relative amount of each nucleotide incorporated against X = G (white), [BTh]G (gray), or [Py]G (black). (c) Primer extension of NarI(22):15mer duplex by Dpo4 (20 nM) where X = G, [BTh]G, or [Py]G. Aliquots (5 μL) of the reactions were removed and quenched in stop dye at each of the time points indicated under each lane. Green triangles indicate base incorporation products that migrate with the unmodified template product, while red triangles indicate base incorporation products with different mobilities on the gel.

adducted G into the major groove (Figures S24 and S32). However, only the *syn* $\theta \sim 0°$ orientation of [BTh]G, and the *syn* θ−180° orientation of [Py]G are energetically accessible (Figure 5a), which differ in the stacking interactions of the C8-moiety (Figures S24 and S32). The pyrene moiety is completely intercalated between the flanking base pairs in [Py]G-adducted DNA and distorts the DNA at the lesion site (Figure S28). The efficient stacking of the pyrene moiety in the helix explains the prominent ICD band for [Py]G adducted DNA. Additionally, the greater DNA distortion resulting from the extrahelical THF explains why [Py]G-adducted DNA has a slightly lower T_m compared to that of the unmodified helix (Table 1). In the case of [BTh]G, only the five-membered heterocyclic ring of the benzothiophene intercalates into the helix, with the six-membered ring being largely solvent exposed in the minor groove. The position of the opposing sugar (THF) is similar to the B-type conformation with [BTh]G paired against C (Figure S20). Taken together, the lower degrees of DNA distortion resulting from the ordered THF residue, concomitant with stacking of the benzothiophene moiety, explains why [BTh]G-adducted DNA has a higher T_m than the unmodified helix (Table 1).

Adducts Paired against the −2 Deletion. The *anti* [BTh]G adduct within the −2 deletion is stabilized by hydrogen bonding with the C in the opposing strand and 5′ with respect to the adduct (Figure S26). The benzothiophene moiety also exhibits favorable stacking interactions with the unpaired C in the major groove. For *syn* ($\theta \sim 0°$) [BTh]G, stabilization of the bulge occurs through stacking between the benzothiophene moiety and the 3′ base pair with respect to the adduct, which does not disrupt Watson−Crick hydrogen bonding in the flanking base pairs. Despite the energetic stabilization of the *anti* ($\theta \sim 180°$) conformation (by 10 kJ mol^{-1}), the *anti* ($\theta \sim 0°$) and *syn* ($\theta \sim 0°$) conformers are likely accessible to the [BTh]G-adducted *Nar*I oligomer paired opposite a 2-base deletion (Figure 5b and Table S3). The greater stabilization of the *anti*-orientation, and only partial stacking of the benzothiophene moiety in the accessible *syn*-conformation, may explain why the ICD band induced by stacking of the C8 moiety is not observed when [BTh]G is paired against a bulge (Figure 2).

In contrast to [BTh]G, the *syn* ($\theta \sim 0°$) conformer is the most stable for [Py]G-adducted DNA (Figure 5b and Table S3). Both *syn*-conformations ($\theta \sim 0°$ and 180°) exhibit sufficient stacking stabilization at the lesion site and are energetically accessible (Table S3). Greater stabilization of the *syn*- compared to the *anti*-conformations, coupled with intercalation of the pyrene moiety in the *syn*-orientations, likely explains the presence of the ICD band and higher T_m of [Py]G-adducted DNA compared to those of the unmodified 2-base bulge (Table 1 and Figure 2).

Primer-Extension of *Nar*I(22). *FLE by Klenow exo$^-$(Kf$^-$).* In the *Nar*I(22) template, the C-linked adducts [Ph]G and [Q]G (Figure 1) were observed previously to block full-length extension by Kf$^-$.[27] Extension one-base past the adduct site was more hindered than incorporation opposite the adduct. A similar result was also previously found for Kf$^-$ extension past [Py]G in a noniterated oligonucleotide template.[37] Bulky N-linked C8-dG adducts also provide significant kinetic barriers to extension by Kf$^-$ following base insertion opposite the adduct.[43] Thus, it was not surprising that [BTh]G and [Py]G strongly blocked extension by Kf$^-$ (Figure S36). For both adducts, incorporation opposite the adduct site (position 1) was possible, but only the primer opposite the template containing [BTh]G was further extended. Extension past [BTh]G was, however, halted after the forth incorporation (position 4). The +8 band observed for extension past X = G (Figure S36) was ascribed to blunt end extension.[27,44]

Translesion Synthesis by Dpo4. Since both [BTh]G and [Py]G blocked extension by Kf$^-$, the model translesion polymerase Dpo4 was used to examine replication of the modified *Nar*I(22) templates. In single-nucleotide incorporation assays (Figure 6a), Dpo4 exhibited low fidelity with the unmodified *Nar*I(22) template (X = G), as observed

DOI: 10.1021/acs.chemrestox.5b00233
Chem. Res. Toxicol. 2015, 28, 1647−1658

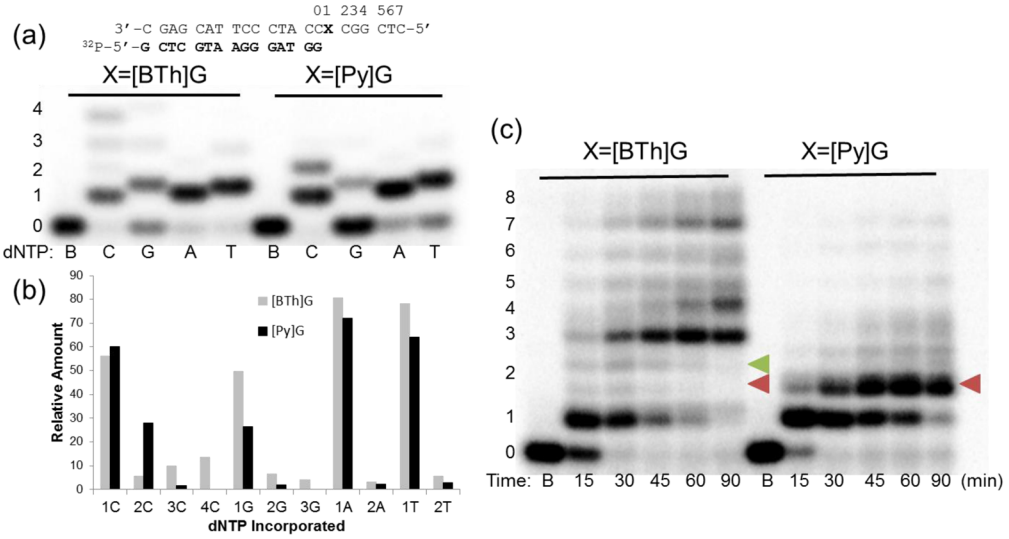

Figure 7. (a) Primer-extension of the *Nar*I(22):15mer duplex (100 nM, X = [BTh]G or [Py]G) by Dpo4 (20 nM) in the presence of individual dNTPs (indicated under each lane, 25 μM) with 20% DMSO in the reaction mixture. Reactions were incubated at 37 °C for 30 min. (b) Relative amount of each nucleotide incorporated against X = [BTh]G (gray) or [Py]G (black). (c) Primer extension of the NarI(22):15mer duplex (X = [BTh]G or [Py]G) by Dpo4 (20 nM) in the presence of 25 μM of each dNTP and 20% DMSO. Aliquots (5 μL) of the reactions were removed and quenched in stop dye at each of the time points indicated under each lane. Green triangles indicate base incorporation products that migrate with the unmodified template product, while red triangles indicate base incorporation products with different mobilities in the gel.

previously.[27] This observation is consistent with its low geometric selection for correct base pairs.[45−48] For base incorporation opposite [BTh]G and [Py]G, the major product of insertion was the correct base C (56% for [BTh]G and 76% for [Py]G), followed by small amounts of A insertion (∼19% for both adducts). Experiments carried out by Kirouac and co-workers on the N-linked aminopyrene ([AP]G) lesion[44] and by Wanninger-Wei*β* on [Py]G in a noniterated sequence[37] yielded similar results.

In the presence of all four dNTPs (Figure 6c), Dpo4 could insert a base opposite the C-linked adducts (presumably C, Figure 7a) but could not extend beyond that (position 1) with any degree of efficiency. This observation differed from our previous primer-extension experiments utilizing [Fur]G-, [Ph]G-, and [Q]G-modified *Nar*I(22), in which Dpo4 could readily extend the 15mer primers past position 1.[27] Of the previously studied C-linked adducts, the strongest block was the bent [Q]G adduct, which blocked extension by Dpo4 at position 3.[27] Thus, the results presented in Figure 6c suggested that the linear-extended C8-aryl rings of [BTh]G and [Py]G played a key role in the observed blockage at position 1. For N-linked C8-dG adducts that block Dpo4 extension following base insertion opposite the adduct, it is predicted that the bulky N-linked C8-aryl group interacts with the little finger domain of the polymerase, which impedes translocation.[49]

In addition to the strong bands at position 1 in Figure 6c, a faint band representing the full-length product was detected at 90 min for Dpo4 extension past [BTh]G. Dpo4 was also stalled at position 3 with the template containing X = [BTh]G. Both modified templates generated multiple faint bands at position 2, which was not observed with the unmodified template, suggesting incorrect (indicated by red triangles) and correct (indicated by green triangles) extension.

Addition of organic solvents (such as 20% DMSO) to primer-elongation reactions has previously been shown to relieve polymerase stalling past the bulky lipophilic N-linked aminopyrene C8-dG adduct ([AP]G).[44] The addition of DMSO decreases the dielectric constant of the aqueous buffer, which is proposed to diminish the adduct-induced stalling effect by stabilizing [AP]G in an *anti*-conformation to allow H-bonding with an opposing base.[44] Thus, primer-extension assays were performed on the modified *Nar*I(22) templates in the presence of 20% DMSO to determine if the nonpolar solvent would increase the extent of replication.

In the presence of individual dNTPs (Figure 7a), the extent of misincorporation opposite [BTh]G and [Py]G in the presence of 20% DMSO strongly increased compared to misincorporation in aqueous buffer (Figure 6a). Opposite [BTh]G misincorporation levels were G (50%), A (80%), and T (78%), while the corresponding levels opposite [Py]G were 26%, 72%, and 64%. When provided with the correct base C, Dpo4 primarily inserted a single C (55% opposite [Bth]G and 60% opposite [Py]G, Figure 7b). However, opposite [BTh]G faint bands for the incorporation of 2 (5%), 3 (8%), or 4 (13%) C bases were observed, while [Py]G promoted incorporation of a second C base (25%). When extension past N-linked C8-dG adducts by Dpo4 at the G3-position of *Nar*I was examined previously,[50] incorporation of a second C was categorized as a two-base slippage phenomenon and implies the pairing of CC with GG one position removed to the 5′-side of the adduct site (positions 3 and 4 in the template strand, Figure 7a). That [Py]G promotes incorporation of a second C suggests that it can induce two-base slippage, which is consistent with its ability to stabilize the 2-base bulge (Table 1). The observation of a band for the incorporation of 4 Cs opposite [BTh]G in *Nar*I(22) suggested slippage and subsequent strand realignment to afford a C:C mismatch at position 2 of the template strand.[27] Both [Fur]G and [Ph]G also induce incorporation of 4 C bases in primer-extension assays with Dpo4.[27]

In the presence of all four dNTPs (Figure 7c), the addition of DMSO permitted the polymerase to extend the template past position 1. Full-length extension past [BTh]G was possible as a band at position 7 was detected after 30 min that grew in intensity over the 90 min incubation. However, even in the

DOI: 10.1021/acs.chemrestox.5b00233
Chem. Res. Toxicol. 2015, 28, 1647−1658

presence of DMSO, position 3 remained a strong block site for Dpo4 extension of the *Nar*I(22) template containing X = [BTh]G. For the template containing X = [Py]G, the presence of 20% DMSO permitted the insertion of a base at position 2, although further extension was blocked at this point. These results suggest that the C-linked [Py]G lesion is a stronger block than the corresponding N-linked derivative, [AP]G.[44]

Given that [BTh]G strongly blocked Dpo4 extension following the incorporation of three bases to afford an 18mer product (position 3, Figure 7c), we were curious to determine if replication by Dpo4 could proceed with the [BTh]G-modified *Nar*I(22) template annealed to 18mer primers (Figure 8). For

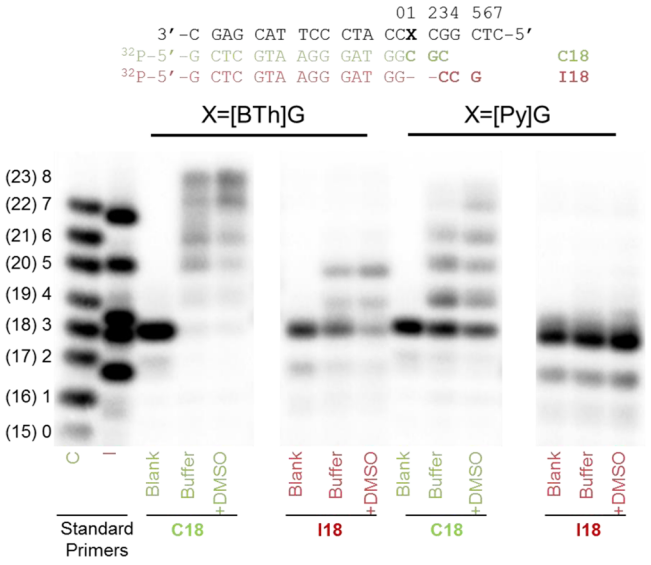

Figure 8. Primer-extension of modified NarI(22):18 mer duplexes (100 nM), containing X = [BTh]G or [Py]G by Dpo4 (20 nm) in the presence of 25 μM dNTPs following incubation for 90 min at 37 °C. The 18mer primers used are listed above the gel in either green for the correct (C18) primer or in red for the incorrect (I18) primer that could induce a 2-base bulge. Extension was run without (buffer) or with 20% DMSO (+DMSO). A blank of each primer was included for comparison, as well as a mixture of correct and incorrect primers (standard primers) of increasing length; see Supporting Information for a detailed description of the various primers (Figure S37).

these experiments, one 18mer primer contained the correct (C18) bases (CGC added to the 15mer, highlighted in green in Figure 8), while the other contained incorrect (I18) bases (CCG added to the 15mer, highlighted in red in Figure 8) that could potentially align with the template strand to induce a 2-base bulge. A full-length 22mer product was detected when the C18 primer was annealed to the template, with or without DMSO in the reaction mixture. Extension past [BTh]G when the I18 primer was annealed showed two bases incorporated to generate a 20mer product, which was fully consistent with a −2 frameshift mutation.[50] These results suggested that the 18mer product produced from Dpo4 extension past [BTh]G (i.e Figure 7c) was neither C19 nor I18, as both primers failed to strongly block the polymerase.

For the [Py]G-modified NarI(22) template, extension past [Py]G by Dpo4 to produce the full-length 22mer product also occurred when the modified template was annealed to the C18 primer (Figure 8). However, no extension was detected when the I18 primer was annealed to the [Py]G-modified *Nar*I(22) template. It was expected that the [Py]G lesion would induce the 2-base bulge with the I18 primer, given its ability to stabilize the truncated duplex within *Nar*I(12) (Table 1). The results presented in Figure 8 suggested that Dpo4 cannot extend past the 2-base bulge containing [Py]G, but it can extend past the bulge containing [BTh]G.

DISCUSSION

Conformational Preferences of C-Linked C8-aryl-dG Adducts within *Nar*I(12) Duplexes. The C8-aryl-dG adducts [Fur]G, [Ph]G, [Q]G,[27] and [BTh]G (Figure 1) favor the major groove B-type structure in *Nar*I(12) paired opposite C, as predicted by MD simulations. Alternative *syn*-conformations are energetically accessible for [Fur]G (higher in energy by 14.2 kJ mol^{-1}),[27] [BTh]G (18.4 kJ mol^{-1}, Figure 3), and most notably [Py]G (7.9 kJ mol^{-1}, Figure 3), while *syn*-conformations for [Ph]G and [Q]G are predicted to be higher in energy than the *anti* orientations by >25 kJ mol^{-1}.[27] The low energy *syn* structures for [Fur]G and [BTh]G adopt the W-type structures with the C8-aryl moiety located in the minor groove. In contrast, the low energy *syn* structure for [Py]G adopts the base displaced intercalated S-type structure (Figure 3), which shares features with the NMR solution S-type structure of [AP]G.[51] Both S-type structures involve complete intercalation of the pyrene moiety into the helix, which displaces the opposing C into the major groove. The strong positive $ICD_{300-400\ nm}$ in the CD spectra (Figure 2) for [Py]G paired opposite C is consistent with the involvement of the S-type structure.[42]

For the adducted *Nar*I(12) oligonucleotides paired with the 10mer (i.e., −2, Table 1) that can produce the −2 deletion duplex, the shape of the aryl system influences duplex stability as additional length projecting away from the guanine base results in [BTh]G and [Py]G stabilizing the truncated duplex (ΔT_m = 3.8 and 6.2, Table 1), in contrast to [Fur]G, Ph[G], and [Q]G.[27] The MD simulations for C-linked C8-dG adducts suggest that bulge stabilization cannot be directly correlated to a *syn* preference of the modified G. For example, *anti* structures are predicted to be more stable than *syn* ones for [Fur]G, Ph[G],[27] and [BTh]G (Figure 5b) by 14.2, 15.1, and 10.0 kJ mol^{-1}, respectively, for which [BTh]G shows bulge stabilization (Table 1). In the low energy *anti* [BTh]G structure ($\theta \sim 180°$, Figure 5b), the benzothiophene moiety exhibits favorable stacking interactions with the unpartnered C in the major groove of the 2-base bulge. In contrast, *syn* structures are predicted to be more stable than *anti* ones for [Q]G[27] and [Py]G (Figure 5b) by 23.8 and 12.6 kJ mol^{-1}, for which [Py]G dramatically stabilizes the −2 deletion duplex (Table 1). In the favored *syn* structures for [Q]G[27] and [Py]G (Figure 5b), the C8-aryl group points toward the minor groove and effectively stacks with the flanking bases that are Watson−Crick hydrogen bonded. The unpartnered C (highlighted in blue, Figure 5b) is positioned in the major groove.

The structural features predicted for the structures containing the C-linked C8-dG adducts differ from those determined for polycyclic N-linked C8-dG adducts.[52,53] For the polycyclic N-linked adducts, the −2 deletion duplexes are bent with the damaged G present in a *syn*-conformation. The N-linked C8-aryl moiety effectively π-stacks with the flanking bases, with damaged G displaced into the major groove. In the NMR solution structure of the −2 deletion duplex containing [AF]G, the unpartnered C is looped out of the helix in the major groove and does not interact with other DNA components.[52] Computational models predict that *anti*

DOI: 10.1021/acs.chemrestox.5b00233
Chem. Res. Toxicol. 2015, 28, 1647−1658

structures are not energetically accessible with much higher energies than *syn* structures (>30 kcal mol^{-1}).[53]

Dpo4 Slippage Mediated by C-Linked C8-aryl-dG Adducts. In SNI assays with the correct base C, the C-linked C8-aryl-dG lesions within *Nar*I(22) induced slippage by Dpo4. In the proposed mechanism outlined in Figure 9, the adducts

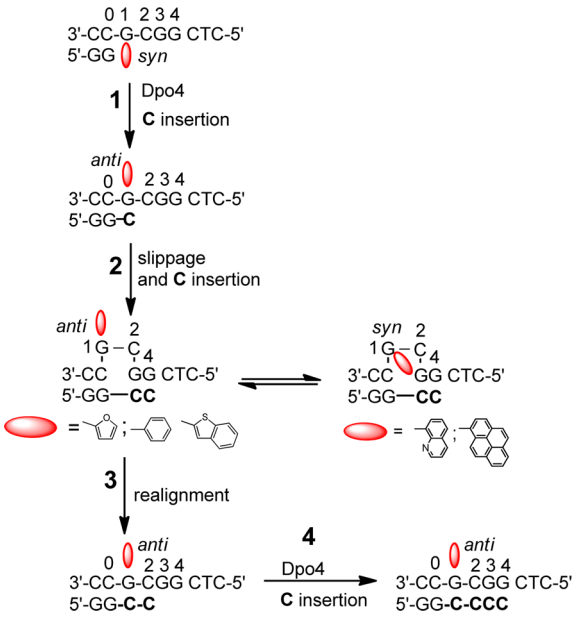

Figure 9. Proposed Dpo4 slippage mechanism induced by C-linked C8-dG adducts within the *Nar*I sequence.

are shown in the *syn*-conformation in the starting template/primer due to the strong *syn* preference of unpaired C-linked C8-dG adducts.[27] Insertion of C (step 1) requires the polymerase to flip the adduct from its stable *syn*-conformation to the energetically destabilized *anti*-conformation. This conformational change is expected to stall DNA replication and permit slippage and production of the 2-base bulge (step 2).[27] Following insertion of a second C opposite G at position 4 in the template strand (included in step 2, Figure 9), the damaged G within the 2-base bulged duplexes can exist as an equilibrium mixture of *anti* and *syn* structures. Our MD simulations predict that [Fur]G, Ph[G],[27] and [BTh]G (Figure 5b) favor the *anti*-conformation, while [Q]G[27] and [Py]G (Figure 5b) favor the *syn*-conformation.

Adducts that favor the *anti*-conformation are predicted to undergo a strand realignment process (step 3) that permits additional C incorporation by Dpo4 (step 4). This mechanism provides a rationale for the incorporation of 4 C bases in the primer-extension assays which generates the C:C mismatch at position 2.[27] For [Fur]G, [Ph]G, and [BTh]G, the levels of 4 C incorporation were 38%, 25%,[27] and 13% (in the presence of 20% DMSO, Figure 7a), respectively. Thus, increased C8-aryl ring size decreased C:C mismatch production.

For [Q]G and [Py]G (Figure 5b), MD simulations favor a *syn*-conformation within the 2-base bulge, which for [Py]G is supported by the positive ICD$_{300-400\ nm}$ band (Figure 2). In primer-extension assays with C, both adducts promoted the incorporation of 2 C bases (40% for [Q]G[27] and 25% for [Py]G (in the presence of 20% DMSO, Figure 7a)), which is classical evidence for 2-base slippage.[50] In the low-energy *syn*-conformation favored by [Q]G[27] and [Py]G (Figure 5b), the adducts within the 2-base bulge are not aligned properly to undergo strand realignment, and thus, both adducts failed to facilitate the incorporation of 4 C bases.

Biological Implications. Our studies provide a model for the mutagenicity of C-linked C8-dG adducts. In general, C-linked C8-dG adducts strongly block DNA replication by Kf$^-$ following the insertion of a single base opposite the lesion (Figure S36).[27,37] Adduct blockage of replicative polymerases *in vivo* is understood to cause polymerase switching, with recruitment of bypass polymerases for translesion synthesis. Translesion polymerases have much lower fidelity than replicative ones and can cause error-prone bypass of DNA adducts to induce mutagenicity.[45−48] Using Dpo4 as a model translesion polymerase, C-linked C8-dG adducts were observed to cause misincorporation (Figures 6a and 7a).[27] Radical cations of B[a]P that can generate the C8−B[*a*]P-dG adduct[12,13] produce G → T and G → C transversion mutations in yeast.[54]

Increased C8-aryl ring size also caused a progressive decrease in full-length extension by Dpo4. For [Py]G and [BTh]G, Dpo4 was strongly blocked after the insertion of a single base opposite the lesion (position 1, Figure 6c). The phenolic fungal toxin ochratoxin A (OTA), which produces a bulky C-linked C8-dG adduct,[14,15,28] affords deletion mutations in the kidney tissue of male rats due to the induction of double-strand breaks.[55,56] Double-stand breaks can occur when a DNA adduct blocks replication by inhibiting the replication fork.[28,57]

In order for C-linked C8-dG adducts to induce mutagenicity, they must evade DNA repair by nucleotide excision repair (NER) enzymes. For the repair of N-linked C8-dG adducts, the [AAF]G lesion is excised by the NER machinery much more efficiently than [AF]G.[58] The greater degree of helix bending/distortion induced by the favored S-type structure produced by *syn*-[AAF]G is regarded as a recognition factor for NER.[59] By analogy, it is anticipated that the bulky C-linked [Py]G lesion will likely be repair prone due to its predicted ability to produce the S-type structure within the *Nar*I duplex (Figure 3). The other C-linked adducts ([Fur]G, [Ph]G, [Q]G,[27] and [BTh]G, Figure 3) that afford the less distorting B-type and W-type structures in the *Nar*I duplex should be less repair prone.

CONCLUSIONS

In the present study, we have examined the structural and biochemical impact of [BTh]G and [Py]G within the *Nar*I sequence. Combined with our previous studies on the corresponding activities for [Fur]G, [Ph]G, and [Q]G,[27] we have now examined how C8-aryl ring size impacts C8-dG adduct conformational preferences and DNA synthesis by Kf$^-$ or Dpo4 for a family of model C-linked C8-dG adducts. Within the *Nar*I(12) duplex, our studies suggest that the bulkiest lesion [Py]G can produce the base-displaced S-type conformation paired opposite C, while all other C-linked adducts favor the B-type structure, which places the C8-aryl ring in the major groove. When hybridized with a truncated 10-mer sequence (−2), only [BTh]G- and [Py]G-modified *Nar*I(12) possessing linearly extended fused C8-aryl rings stabilize the truncated duplex (Table 1), which is regarded as a mimic of the slipped mutagenic product of a 2-base deletion. Computer models suggest that *anti*- and *syn*-conformations of the adduct within the 2-base bulged duplexes possess similar energies with [Py]G favoring the *syn*-conformation (by 12.6 kJ mol^{-1}), while [BTh]G favors the *anti*-conformation (by 10.0 kJ mol^{-1}). These findings differ from 2-base bulged duplex structures

DOI: 10.1021/acs.chemrestox.5b00233
Chem. Res. Toxicol. 2015, 28, 1647−1658

containing polycyclic N-linked C8-dG adducts, which strongly favor the *syn*-conformation (by >30 kcal mol^{-1}). In terms of primer-elongation, our studies demonstrate that increased C8-aryl ring size blocks extension by Kf$^-$ and Dpo4. For the bulkiest lesion [Py]G, Kf$^-$ and Dpo4 can insert a base opposite the adduct but cannot extend beyond that with any degree of efficiency. Our studies also demonstrate that the size of C8-aryl moiety dictates Dpo4 slippage outcome within the CG dinucleotide repeat of the *Nar*I sequence. A model for polymerase slippage mediated by C-linked C8-dG adducts has been derived from adduct conformation within the −2 deletion duplex, as determined using MD simulations. C-Linked adducts that prefer an *anti*-conformation ([Fur]G, [Ph]G, and [BTh]G) are proposed to undergo strand realignment to generate a C:C mismatch distal to the adduct site, while those that prefer a *syn*-conformation ([Q]G and [Py]G) cause 2-base slippage. Future studies dealing with the biochemical influence of C-linked C8-dG adducts within the *Nar*I(22) template will employ additional Y-polymerase enzymes to determine which polymerase may extend the bulky C-linked C8-dG base pair. Here, we intend to include kinetic assays to provide a quantitative measure of the nucleotide selection preferences of Y-family polymerases opposite the C-linked C8-dG adducts and use LC-MS to sequence the extension products. In terms of structural impact of C-linked C8-dG adducts, our CD, fluorescence, and MD structural data should be confirmed in future studies with NMR and/or X-ray crystallography. Lastly, C-linked C8-dG adducts of defined structure have yet to be incorporated into DNA vectors for the determination of mutational frequency in cell-based assays. Thus, it would also be interesting to make a direct comparison between the mutagenicity of [Py]G with [AP]G in a cell-based assay so that the biological impact of linkage type (C- vs N-) can be established for C8-dG adducts.

■ ASSOCIATED CONTENT

Supporting Information

The Supporting Information is available free of charge on the ACS Publications website at DOI: 10.1021/acs.chemrestox.5b00233.

Synthetic and computational details, NMR spectra of phosphoramidites, MS analysis of modified *Nar*I oligonucleotides, primer-extension of modified *Nar*I(22) templates by Kf$^-$, and full description of the MD simulation procedure and results
(PDF)

■ AUTHOR INFORMATION

Corresponding Authors

*(R.A.M.) Tel: 1-519-824-4120 ext. 53963. E-mail: rmanderv@uoguelph.ca;
*(S.D.W.) Tel: 1-403-329-2323. E-mail: stacey.wetmore@uleth.ca.

Present Address

§P.S.: Center for Computational Sciences, Central University of Punjab, Bathinda, Punjab, 151001, India.

Funding

This work was supported by the Natural Sciences and Engineering Research Council of Canada (Discovery grants to R.A.M, 311600-2013, and S.D.W., 249598-07); and the Canada Research Chain Program (S.D.W., 950-228175).

Notes

The authors declare no competing financial interest.

■ ACKNOWLEDGMENTS

Computational resources provided by Westgrid and Compute/Calcul Canada are greatly appreciated.

■ ABBREVIATIONS

dG, 2′-deoxyguanosine; [BTh]G, C8- benzo[*b*]thienyl-dG; [Py]G, C8-(pyren-1-yl)-dG; CD, circular dichroism; MD, molecular dynamics

■ REFERENCES

(1) Luch, A. (2005) Nature and nurture − lessons from chemical carcinogenesis. *Nat. Rev. Cancer 5*, 113−125.
(2) Millen, A. L., Sharma, P., and Wetmore, S. D. (2012) C8-linked bulky guanosine DNA adducts: Experimental and computational insights into adduct conformational preferences and resulting mutagenicity. *Future Med. Chem. 4*, 1981−2007.
(3) Beland, F. A., and Kadlubar, F. F. (1990) Chemical Carcinogenesis and Mutagenesis, in *Handbook of Experimental Pharmacology* (Cooper, C. S., and Grover, P. L., Eds.) Vol. *94/I*, pp 267−325, Springer-Verlag, Heidelberg, Germany.
(4) Purohit, V., and Basu, A. K. (2000) Mutagenicity of nitroaromatic compounds. *Chem. Res. Toxicol. 13*, 673−692.
(5) Turesky, R. J. (2002) Heterocyclic aromatic amine metabolism, DNA adduct formation, mutagenesis, and carcinogenesis. *Drug Metab. Rev. 34*, 625−650.
(6) Patel, D. J., Mao, B., Gu, Z., Hingerty, B. E., Gorin, A., Basu, A. K., and Broyde, S. (1998) Nuclear magnetic resonance solution structures of covalent aromatic amine−DNA adducts and their mutagenic relevance. *Chem. Res. Toxicol. 11*, 391−407.
(7) Cho, B. P. (2004) Dynamic conformational heterogeneities of carcinogen-DNA adducts and their mutagenic relevance. *J. Environ. Sci. Heal. C 22*, 57−90.
(8) Hiramoto, K., Kaku, M., Sueyoshi, A., Fujise, M., and Kikugawa, K. (1995) DNA base and deoxyribose modification by the carbon-centered radical generated from 4-(hydroxymethyl) benzenediazonium salt, a carcinogen in mushroom. *Chem. Res. Toxicol. 8*, 356−362.
(9) Train, B. C., Bilgesü, S. A., Despeaux, E. C., Vongsutilers, V., and Gannett, P. M. (2014) Single C8-arylguanine modifications render oligonucleotides in the Z-DNA conformation under physiological conditions. *Chem. Res. Toxicol. 27*, 1176−1186.
(10) Akanni, A., and AbulHajj, Y. J. (1997) Estrogen nucleic acid adducts: reaction of 3,4-estrone-o-quinone radical anion with deoxyribonucleosides. *Chem. Res. Toxicol. 10*, 760−766.
(11) Akanni, A., and Abul-Hajj, Y. J. (1999) Estrogen-nucleic acid adducts: dissection of the reaction of 3,4-estrone quinone and its radical anion and radical cation with deoxynucleosides and DNA. *Chem. Res. Toxicol. 12*, 1247−1253.
(12) Rogan, E. G., Cavalieri, E. L., Tibbels, S. R., Cremonesi, P., Warner, C. D., Nagel, D. L., Tomer, K. B., Cerney, R. L., and Gross, M. L. (1988) Synthesis and identification of benzo[a]pyrene-guanine nucleoside adducts formed by electrochemical oxidation and by horseradish peroxidase catalyzed reaction of benzo[a]pyrene with DNA. *J. Am. Chem. Soc. 110*, 4023−4029.
(13) Dai, Q., Xu, D., Lim, K., and Harvey, R. G. (2007) Efficient syntheses of C8-aryl adducts of adenine and guanine formed by reaction of radical cation metabolites of carcinogenic polycyclic aromatic hydrocarbons with DNA. *J. Org. Chem. 72*, 4856−4863.
(14) Dai, J., Wright, M. W., and Manderville, R. A. (2003) Ochratoxin A forms a carbon-bonded C8-deoxyguanosine nucleoside adduct: implications for C8 reactivity by a phenolic radical. *J. Am. Chem. Soc. 125*, 3716−3717.
(15) Mantle, P. G., Faucet-Marquis, V., Manderville, R. A., Squillaci, B., and Pfohl-Leszkowicz, A. (2010) Structures of covalent adducts between DNA and ochratoxin A: a new factor in debate about

DOI: 10.1021/acs.chemrestox.5b00233
Chem. Res. Toxicol. 2015, 28, 1647−1658

genotoxicity and human risk assessment. *Chem. Res. Toxicol. 23*, 89−98.
(16) Manderville, R. A. (2009) Structural and Biological Impact of Radical Addition Reactions with DNA Nucleobases, in *Advances in Physical Organic Chemistry* (Richard, J. P., Ed.) pp 177−218, Elsevier, Amsterdam.
(17) Kuska, M. S., Witham, A. A., Sproviero, M., Manderville, R. A., Majdi Yazdi, M., Sharma, P., and Wetmore, S. D. (2013) Structural influence of C8-phenoxy-guanine in the *Nar*I recognition DNA sequence. *Chem. Res. Toxicol. 26*, 1397−1408.
(18) Witham, A. A., Verwey, A. M. R., Sproviero, M., Manderville, R. A., Sharma, P., and Wetmore, S. D. (2015) Chlorine functionalization of a model phenolic C8-guanine adduct increases conformational rigidity and blocks extension by a Y-family DNA polymerase. *Chem. Res. Toxicol. 28*, 1346−1356.
(19) Manderville, R. A. (2005) Ambident reactivity of phenoxyl radicals in DNA adduction. *Can. J. Chem. 83*, 1261−1267.
(20) Cho, B. P., Beland, F. A., and Marques, M. M. (1992) NMR structural studies of a 15-mer DNA sequence from ras protooncogene modified at the first base of codon 61 with the carcinogen 4-aminobiphenyl. *Biochemistry 31*, 9587−9602.
(21) Mao, B., Hingerty, B. E., Broyde, S., and Patel, D. J. (1998) Solution structure of the aminofluorene [AF]-intercalated conformer of the *syn*-[AF]-C8-dG adduct opposite dC in a DNA duplex. *Biochemistry 37*, 81−94.
(22) Wang, F., DeMuro, N. E., Elmquist, C. E., Stover, J. S., Rizzo, C. J., and Stone, M. P. (2006) Base-displaced intercalated structure of the food mutagen 2-amino-3-methylimidazo[4,5-*f*]quinoline in the recognition sequence of the *Nar*I restriction enzyme, a hotspot for − 2 bp deletions. *J. Am. Chem. Soc. 128*, 10085−10095.
(23) Shapiro, R., Hingerty, B. E., and Broyde, S. (1989) Minor-groove binding models for acetylaminofluorene modified DNA. *J. Biomol. Struct. Dyn. 7*, 493−513.
(24) Elmquist, C. E., Wang, F., Stover, J. S., Stone, M. P., and Rizzo, C. J. (2007) Conformational differences of the C8-deoxyguanosine adduct of 2-amino-3-methylimidazo[4,5-*f*]quinoline (IQ) within the *Nar*I recognition sequence. *Chem. Res. Toxicol. 20*, 445−454.
(25) Wang, F., Elmquist, C. E., Stover, J. S., Rizzo, C. J., and Stone, M. P. (2007) DNA sequence modulates the conformation of the food mutagen 2-amino-3-methylimidazo[4,5-*f*]quinoline in the recognition sequence of the *Nar*I restriction enzyme. *Biochemistry 46*, 8498−8516.
(26) Cho, B. (2010) Structure-Function Characteristics of Aromatic Amine-DNA Adducts, in *The Chemical Biology of DNA Damage* (Geacintov, N. E., and Broyde, S., Eds.) pp 217−238, Wiley-VCH Verlag GmbH & Co. KGaA, Weinheim, Germany.
(27) Sproviero, M., Verwey, A. M. R., Rankin, K. M., Witham, A. A., Soldatov, D. V., Manderville, R. A., Fekry, M. I., Sturla, S. J., Sharma, P., and Wetmore, S. D. (2014) Structural and biochemical impact of C8-aryl-guanine adducts within the *Nar*I recognition DNA sequence: influence of aryl ring size on targeted and semi-targeted mutagenicity. *Nucleic Acids Res. 42*, 13405−13421.
(28) Sharma, P., Manderville, R. A., and Wetmore, S. D. (2014) Structural and energetic characterization of the major DNA adduct formed from the food mutagen ochratoxin A in the *Nar*I hotspot sequence: influence of adduct ionization on the conformational preferences and implications for the NER propensity. *Nucleic Acids Res. 42*, 11831−11845.
(29) Sharma, P., Majdi Yazdi, M., Merriman, A., Manderville, R. A., and Wetmore, S. D. (2015) Influence of the linkage type and functional groups in the carcinogenic moiety on the conformational preferences of damaged DNA: structural and energetic characterization of carbon- and oxygen-linked C8 phenolic-guanine adducts. *Chem. Res. Toxicol. 28*, 782−796.
(30) Fuchs, R. P. P., Schwartz, N., and Daune, M. P. (1981) Hot spots of frameshift mutations induced by the ultimate carcinogen *N*-acetoxy-*N*-2-acetylaminofluorene. *Nature 294*, 657−659.
(31) Hoffmann, G. R., and Fuchs, R. P. P. (1997) Mechanisms of frameshift mutations: insight from aromatic amines. *Chem. Res. Toxicol. 10*, 347−359.
(32) Zhou, Y., and Romano, L. J. (1993) Solid-phase synthesis of oligonucleotides containing site-specific N-(2′-deoxyguanosin-8-yl)-2-(acetylamino)fluorene adducts using 9-fluorenylmethoxycarbonyl as the base-protecting group. *Biochemistry 32*, 14043−14052.
(33) Milhe, C., Fuchs, R. P. P., and Lefevre, J. F. (1996) NMR data show that the carcinogen N-2-acetylaminofluorene stabilises an intermediate of − 2 frameshift mutagenesis in a region of high mutation frequency. *Eur. J. Biochem. 235*, 120−127.
(34) Elmquist, C. E., Stover, J. S., Wang, Z., and Rizzo, C. J. (2004) Site-specific synthesis and properties of oligonucleotides containing C8-deoxyguanosine adducts of the dietary mutagen IQ. *J. Am. Chem. Soc. 126*, 11189−11201.
(35) Rankin, K. M., Sproviero, M., Rankin, K., Sharma, P., Wetmore, S. D., and Manderville, R. A. (2012) C8-heteroaryl-2′-deoxyguanosine adducts as conformational fluorescent probes in the *Nar*I recognition sequence. *J. Org. Chem. 77*, 10498−10508.
(36) Valis, L., Mayer-Enthart, E., and Wagenknecht, H.-A. (2006) 8-(Pyren-1-yl)-2′-deoxyguanosine as an optical probe for DNA hybridization and for charge transfer with small peptides. *Bioorg. Med. Chem. Lett. 16*, 3184−3187.
(37) Wanninger-Weiß, C., Di Pasquale, F., Ehrenschwender, T., Marx, A., and Wagenknecht, H.-A. (2008) Nucleotide insertion and bypass synthesis of pyrene- and BODIPY-modified oligonucleotides by DNA polymerases. *Chem. Commun.*, 1443−1445.
(38) Western, E. C., Daft, J. R., Johnson, E. M., II, Gannett, P. M., and Shaughnessy, K. H. (2003) Efficient one-step Suzuki arylation of unprotected halonucleosides using water-soluble palladium catalysts. *J. Org. Chem. 68*, 6767−6774.
(39) Verwey, A. M. R., Witham, A. A., Li, M., and Manderville, R. A. (2014) Mutagenicity analysis of C8-phenoxy-guanine in the *Nar*I recognition DNA sequence. *J. Toxins 1*, 6.
(40) Takeshita, M., Chang, C. N., Johnson, F., Will, S., and Grollman, A. P. (1987) Oligodeoxynucleotides containing synthetic abasic sites. Model substrates for DNA polymerases and apurinic/apyrimidinic endonucleases. *J. Biol. Chem. 262*, 10171−10179.
(41) Gray, D. M., Ratliff, R. L., and Vaughan, M. R. (1992) Circular dichroism spectroscopy of DNA. *Methods in Enzymol. 211*, 389−406.
(42) Jain, N., Li, Y., Zhang, L., Meneni, S. R., and Cho, B. P. (2007) Probing the sequence effects of *Nar*I-induced − 2 frameshift mutagenesis by dynamic ^{19}F NMR, UV, and CD spectroscopy. *Biochemistry 46*, 13310−13321.
(43) Miller, H., and Grollman, A. P. (1997) Kinetics of DNA polymerase I (Klenow fragment exo-) activity on damaged DNA templates: effect of proximal and distal template damage on DNA synthesis. *Biochemistry 36*, 15336−15342.
(44) Kirouac, K. N., Basu, A. K., and Ling, H. (2013) Structural mechanism of replication stalling on a bulky amino-polycyclic aromatic hydrocarbon DNA adduct by a Y-family DNA polymerase. *J. Mol. Biol. 425*, 4167−4176.
(45) Ling, H., Boudsocq, F., Woodgate, R., and Yang, W. (2001) Crystal structure of a Y-family DNA polymerase in action: a mechanism for error-prone and lesion-bypass replication. *Cell 107*, 91−102.
(46) Broyde, S., Wang, L., Rechkoblit, O., Geacintov, N. E., and Patel, D. J. (2008) Lesion processing: high-fidelity versus lesion-bypass DNA polymerases. *Trends Biochem. Sci. 33*, 209−219.
(47) Lange, S. S., Takata, K., and Wood, R. D. (2011) DNA polymerases and cancer. *Nat. Rev. Cancer 11*, 96−110.
(48) Kokoska, R. J., Bebenek, K., Boudsocq, F., Woodgate, R., and Kunkel, T. A. (2002) Low fidelity DNA synthesis by a Y family DNA polymerase due to misalignment in the active site. *J. Biol. Chem. 277*, 19633−19638.
(49) Wang, L., and Broyde, S. (2006) A new *anti* conformation for *N*-(deoxyguanosin-8-yl)-2-acetylaminofluorene (AAF-dG) allows Watson-Crick pairing in the *Sulfolobus solfataricus* P2 DNA polymerase IV (Dpo4). *Nucleic Acids Res. 34*, 785−795.
(50) Stover, J. S., Chowdhury, G., Zang, H., Guengerich, F. P., and Rizzo, C. J. (2006) Translesion synthesis past the C8- and N^2-deoxyguanosine adducts of the dietary mutagen 2-amino-3-

DOI: 10.1021/acs.chemrestox.5b00233
Chem. Res. Toxicol. 2015, 28, 1647−1658

methylimidazo[4,5-f]quinoline in the *Nar*I recognition sequence by prokaryotic DNA polymerases. *Chem. Res. Toxicol. 19*, 1506−1517.
(51) Mao, B., Vyas, R. R., Hingerty, B. E., Broyde, S., Basu, A. K., and Patel, D. J. (1996) Solution conformation of the N-(deoxyguanosin-8-yl)-1-aminopyrene ([AP]dG) adduct opposite dC in a DNA duplex. *Biochemistry 35*, 12659−12670.
(52) Mao, B., Gorin, A., Gu, Z., Hingerty, B. E., Broyde, S., and Patel, D. J. (1997) Solution structure of the aminofluorene-intercalated conform of the syn [AF]-C8-dG adduct opposite a −2 deletion site in the *Nar*I hot spot sequence context. *Biochemistry 36*, 14479−14490.
(53) Roy, D., Hingerty, B. E., Shapiro, R., and Broyde, S. (1998) A slipped replication intermediate model is stabilized by the syn orientation of *N*-2-aminofluorene- and *N*-2-(acetyl)aminofluorene-modified guanine at a mutational hotspot. *Chem. Res. Toxicol. 11*, 1301−1311.
(54) Sen, S., Bhojnagarwala, P., Francey, L., Lu, D., Penning, T. M., and Field, J. (2012) p53 mutagenesis by benzo[a]pyrene derived radical cations. *Chem. Res. Toxicol. 25*, 2117−2126.
(55) Hibi, D., Suzuki, Y., Ishii, Y., Jin, M., Watanabe, M., Sugita-Konishi, Y., Yanai, T., Nohmi, T., Nishikawa, A., and Umemura, T. (2011) Site-specific in vivo mutagenicity in the kidney of gpt delta rats given a carcinogenic dose of ochratoxin A. *Toxicol. Sci. 122*, 406−414.
(56) Hibi, D., Kijima, A., Kuroda, K., Suzuki, Y., Ishii, Y., Jin, M., Nakajima, M., Sugita-Konishi, Y., Yanai, T., Nohmi, T., Nishikawa, A., and Umemura, T. (2013) Molecular mechanisms underlying ochratoxin A-induced genotoxicity: global gene expression analysis suggests induction of DNA double-strand breaks and cell cycle progression. *J. Toxicol. Sci. 38*, 57−69.
(57) Bi, X., Slater, D. M., Ohmori, H., and Vaziri, C. (2005) DNA polymerase κ is specifically required for recovery from the benzo[a]-pyrene-dihydrodiol epoxide (BPDE)-induced s-phase checkpoint. *J. Biol. Chem. 280*, 22343−22355.
(58) Gillet, L. C., Alzeer, J., and Scharer, O. D. (2005) Site-specific incorporation of N-(deoxyguanosin-8-yl)-2-acetylaminofluorene (dG-AAF) into oligonucleotides using modified 'ultra-mild' DNA synthesis. *Nucleic Acids Res. 33*, 1961−1969.
(59) Jain, V., Hilton, B., Lin, B., Patnaik, S., Liang, F., Darian, E., Zou, Y., MacKerell, A. D., Jr, and Cho, B. P. (2013) Unusual sequence effects on nucleotide excision repair of arylamine lesions: DNA bending/distortion as a primary recognition factor. *Nucleic Acids Res. 41*, 869−880.

DOI: 10.1021/acs.chemrestox.5b00233
Chem. Res. Toxicol. 2015, 28, 1647−1658